AIAA 93-0065

A Solution Scheme for the Euler Equations Based on a Multi-Dimensional Wave Model

K. G. Powell
The University of Michigan
Ann Arbor, MI

T. J.Barth
NASA Ames Research Center
MoffetField, CA

I. H. Parpia
The University of Texas at Arlington
Arlington, TX

31st Aerospace Sciences Meeting & Exhibit
January 11-14, 1993 / Reno, NV

A Solution Scheme for the Euler Equations Based on a Multi-Dimensional Wave Model

Kenneth G. Powell*
University of Michigan
Ann Arbor, MI

Timothy J. Barth†
NASA Ames Research Center
Moffet Field, CA

Ijaz H. Parpia‡
University of Texas, Arlington
Arlington, TX

January, 1993

Abstract

A scheme for the solution of scalar advection on an unstructured mesh has been developed, tested, and extended to the Euler equations. The scheme preserves a linear function exactly, and yields nearly monotone results. The flux function associated with the Euler scheme is based on a discrete "wave model" for the system of equations. The wave model decomposes the solution gradient at a location into shear waves, entropy waves and acoustic waves and calculates the speeds, strengths and directions associated with the waves. The approach differs from typical flux-difference splitting schemes in that the waves are not assumed to propagate normal to the faces of the control volumes; directions of propagation of the waves are instead computed from solution-gradient information. Results are shown for three test cases, and two different wave models. The results are compared to those from other approaches, including MUSCL and Galerkin least squares schemes.

Introduction

Algorithms for solving the Euler equations on unstructured grids are achieving a high level of sophistication. In particular, upwind methods for computation of compressible flows have advanced dramatically from the days of linear schemes which were inherently first-order accurate. One substantial improvement in solution accuracy on unstructured meshes has been obtained by using high order polynomial representations of the solution data [Bar90, BF90], coupled with nonlinear limiter functions, to achieve schemes that are very accurate in smooth regions of the flow without introducing oscillations in regions of high gradients of the solution. It has also been shown that solution accuracy can be improved if a more careful accounting is taken of the wave structure inherent in the Euler equations [PM92, PvLR90, SDD+91]. This is achieved by computing wave directions and strengths from a wave model, rather than postulating that the waves move perpendicular to the cell-faces of the mesh. In the work presented here, an attempt is made to merge these two improvements in a single unified scheme for high-order accurate solution of the Euler equations on unstructured meshes.

The present scheme assumes an unstructured mesh, with the conserved variables stored at vertices. Recent work on multi-dimensional schemes for scalar advection on ustructured meshes has concen-

*Assistant Professor, Aerospace Engineering, AIAA Senior Member

†Research Scientist, Computational Fluid Dynamics, AIAA Senior Member

‡Assistant Professor, Mechanical/Aerospace Engineering, AIAA Senior Member

trated on a cell-vertex, or "fluctuation-splitting" approach [DSPR91, DSR90], or on a MUSCL-type approach [vL79] on a structured mesh [Sid89, RS91]. In the work presented here, a flux-based finite-volume scheme that is well-suited for use on unstructured meshes is developed. An edge-based data structure [Bar90] is used, with edge-to-vertex and edge-to-triangle connectivity stored. Fluxes are computed through faces of the median-dual mesh, and summed to compute the residuals associated with cells of the dual mesh. The changes in time are integrated by a multi-stage procedure.

The Solution Algorithm

The solution algorithm is composed of four pieces, which are described below. They are:

- An accurate, nearly monotone finite-volume scheme for computing scalar advection on an unstructured mesh;
- A wave model for determining the strengths and directions and speeds of propagation of the waves;
- A flux function based on the derived wave strengths, speeds and directions, and consistent with the scalar advection scheme;
- A reconstruction technique for increasing the order of accuracy of the scheme.

A Multi-Dimensional Scheme for Scalar Advection

The basis of the Euler scheme is a finite-volume scheme for scalar advection which uses information about the solution-gradient direction to minimize the dissipation. The scheme is vertex-based, with changes in a scalar quantity u at a vertex computed by calculating fluxes through the faces of the corresponding cell of the centroid-dual mesh (see Figure 1).

The simplest scheme for discretizing a scalar advection equation

$$\frac{\partial u}{\partial t} + \boldsymbol{\lambda} \cdot \nabla u = 0 \tag{1}$$

on this type of mesh is the Galerkin scheme, which may be written as

$$\frac{\partial u_0}{\partial t} = -\frac{1}{A_0} \sum_{i=1}^{n_{edges}} \boldsymbol{\lambda} \cdot \mathbf{n}_i \frac{u_i + u_0}{2} , \tag{2}$$

where A_0 is the area of the dual cell, $\mathbf{n}_i$ is the normal corresponding to the i^{th} face of the dual cell, and u_i

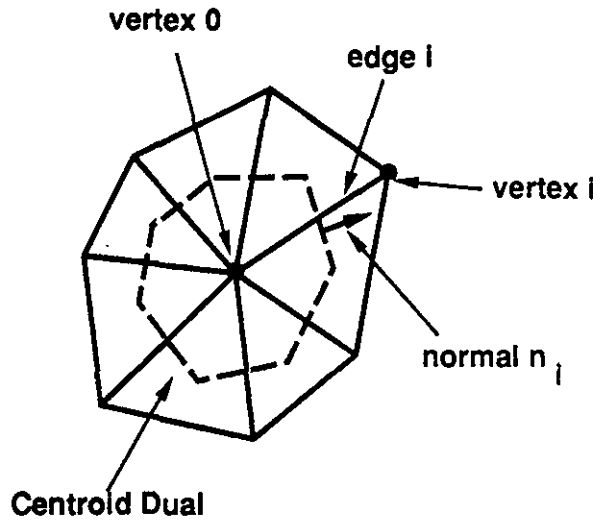

Figure 1: Vertex Mesh and the Centroid Dual

denotes the value of the scalar quantity u at vertex i, as depicted in Figure 1.

Two properties that are desirable in a scheme for scalar advection are positivity and linearity preservation. Whether or not a scheme has these properties can be determined by writing the scheme in the form

$$u_0^{n+1} = u_0^n + \Delta t \sum_{i=0}^{n_{edges}} c_i u_i^n , \tag{3}$$

and examining the c_i's. Positivity is desirable from the point of view of stability and monotonicity; a scheme that is positive is stable in a maximum norm, and will capture flow discontinuitites without oscillations. For positivity, the requirement is that

$$1 + \Delta t c_0 \geq 0 \tag{4a}$$

$$c_i \geq 0 . \tag{4b}$$

For linearity preservation, the requirement is that

$$\sum_{i=0}^{n_{edges}} c_i x_i = -\lambda_x \tag{5a}$$

$$\sum_{i=0}^{n_{edges}} c_i y_i = -\lambda_y . \tag{5b}$$

Linearity preservation is desirable from the point of view of accuracy; a linearity-preserving scheme on a uniform mesh would be second-order accurate.

For the Galerkin scheme,

$$c_0 = -\frac{1}{2A_0} \sum_{i=1}^{n_{edges}} \boldsymbol{\lambda} \cdot \mathbf{n}_i \tag{6a}$$

$$c_i = -\frac{1}{2A_0}\boldsymbol{\lambda}\cdot\mathbf{n}_i \,. \qquad (6b)$$

The Galerkin scheme does not meet the positivity constraint for any value of Δt. It does, however, meet the constraint for linearity preservation.

The simplest positive scheme is the first-order upwind scheme, which can be written as

$$\frac{\partial u_0}{\partial t} = -\frac{1}{A_0}\sum_{i=1}^{n_{edges}}\left[\boldsymbol{\lambda}\cdot\mathbf{n}_i\frac{u_i+u_0}{2} - |\boldsymbol{\lambda}\cdot\mathbf{n}_i|\frac{u_i-u_0}{2}\right], \qquad (7)$$

corresponding to coefficients

$$c_0 = -\frac{1}{2A_0}\sum_{i=1}^{n_{edges}}\left[\boldsymbol{\lambda}\cdot\mathbf{n}_i + |\boldsymbol{\lambda}\cdot\mathbf{n}_i|\right] \qquad (8a)$$

$$c_i = -\frac{1}{2A_0}\left[\boldsymbol{\lambda}\cdot\mathbf{n}_i - |\boldsymbol{\lambda}\cdot\mathbf{n}_i|\right], \qquad (8b)$$

which may be interpreted as the Galerkin scheme (the $\boldsymbol{\lambda}\cdot\mathbf{n}_i$ terms) with added dissipation (the $|\boldsymbol{\lambda}\cdot\mathbf{n}_i|$ terms). This scheme is positive, subject to the CFL condition

$$\Delta t < \frac{A}{\sum_{i=1}^{n_{edges}}(\boldsymbol{\lambda}\cdot\mathbf{n}_i)_{positive}} \qquad (9)$$

It is not, however, linearity-preserving. A result for a circular convection problem for this scheme is shown in Figure 2; the spreading of the contours shows the low accuracy of the scheme. The grid for this test case is shown in Figure 3.

The two schemes described above demonstrate the difficulty inherent in designing a positive, accurate scheme. To design a scheme that meets both criteria, the scheme must be made nonlinear. One way to introduce nonlinearity into the scheme is to use solution-gradient information, making use of the fact that

$$\boldsymbol{\lambda}\cdot\nabla u = \boldsymbol{\lambda}^*\cdot\nabla u \qquad (10)$$

where

$$\boldsymbol{\lambda}^* = \boldsymbol{\lambda}\cdot\mathbf{k}\,\mathbf{k} \qquad (11)$$

and

$$\mathbf{k} = \frac{\nabla u}{|\nabla u|} \,. \qquad (12)$$

This is a statement of the fact that, in terms of wave propagation, it is not simply the convection speed and direction that are important; the solution gradient direction must be taken into account. As illustrated in Figure 4, the perceived wave motion is not that given by the convection velocity ($\boldsymbol{\lambda}$), but that given

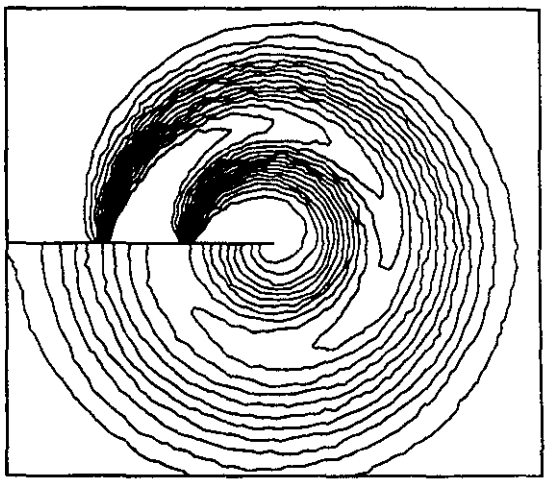

Figure 2: Circular Convection Results — First-Order Upwind Scheme

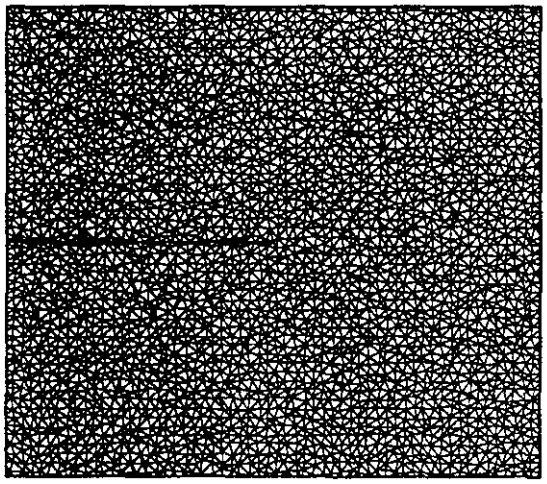

Figure 3: Circular Convection Results — Grid

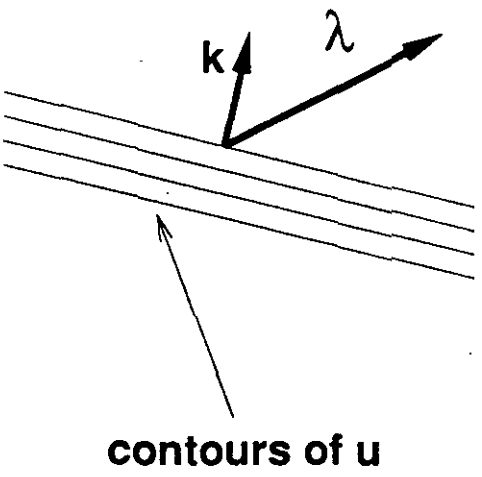

Figure 4: Role of the Convection and Solution-Gradient Directions in Wave Propagation

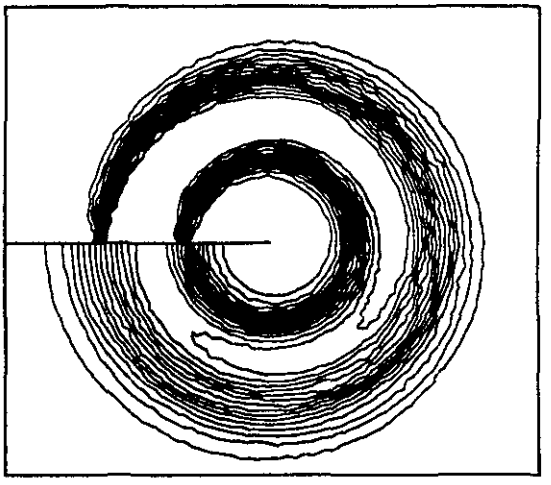

Figure 5: Circular Convection Results — Nonlinear Upwind Scheme

by the projection of the convection velocity on the solution gradient direction ($\boldsymbol{\lambda}^*$).

Using the equivalence defined in Equation 10, then, a modified Galerkin scheme

$$\frac{\partial u_0}{\partial t} = -\frac{1}{A_0} \sum_{i=1}^{n_{edges}} \boldsymbol{\lambda}^* \cdot \mathbf{n}_i \frac{u_i + u_0}{2} , \qquad (13)$$

should give the same solution for u as the Galerkin scheme defined in Equation 2. For now, the issue of how the discrete approximation to ∇u, used to form $\boldsymbol{\lambda}^*$, will not be discussed in detail. It should be noted, however, that the discrete approximation to $\boldsymbol{\lambda}^*$ affects the monotonicity of the scheme, and more work remains to be done to find the best way to calculate $\boldsymbol{\lambda}^*$. Once a modified Galerkin scheme has been written in this way, it is clear that an upwind-biased scheme with less dissipation than that of Equation 7 may be constructed, which still meets the positivity constraint. The scheme is

$$\frac{\partial u_0}{\partial t} = -\frac{1}{A_0} \sum_{i=1}^{n_{edges}} \left[\boldsymbol{\lambda}^* \cdot \mathbf{n}_i \frac{u_i + u_0}{2} - |\boldsymbol{\lambda} \cdot \mathbf{k}\, \mathbf{k} \cdot \mathbf{n}_i| \frac{u_i - u_0}{2} \right] , \qquad (14)$$

or, since the the distinction between $\boldsymbol{\lambda}$ and $\boldsymbol{\lambda}^*$ is unimportant in the Galerkin portion of the scheme,

$$\frac{\partial u_0}{\partial t} = -\frac{1}{A_0} \sum_{i=1}^{n_{edges}} \left[\boldsymbol{\lambda} \cdot \mathbf{n}_i \frac{u_i + u_0}{2} - |\boldsymbol{\lambda} \cdot \mathbf{k}\, \mathbf{k} \cdot \mathbf{n}_i| \frac{u_i - u_0}{2} \right] . \qquad (15)$$

From the scheme written in the form of Equation 14, it is easy to see that the scheme meets the constraint of linearity preservation; the Galerkin term preserves a linear function, and the dissipation term ultimately disappears for a linear function, since $\boldsymbol{\lambda} \perp \nabla u$ in the steady state. It is interesting to note two special cases:

- if $\nabla u \perp \mathbf{n}$, the scheme reverts to the Galerkin scheme;
- if $\nabla u \parallel \mathbf{n}$, the scheme reverts to the full upwind scheme.

It is not as easy to prove positivity, because of the dependence on the way that $\boldsymbol{\lambda}^*$ is calculated. Numerical results are nearly monotone, however. Results for the circular convection case are shown in Figure 5; they are appreciably less diffused than those of Figure 2, and are non-oscillatory.

Nonlinearity is typically introduced into upwind schemes by a limited reconstruction step, such as that described by Barth [Bar90]. The results shown in Figure 6 are for the upwind scheme of Equation 7 combined with a limited linear reconstruction. Results for a combination of the scheme of Equation 15 and the same reconstruction operator are shown in Figure 7. Finally, for comparison, results for the NN fluctuation-splitting scheme [DSPR91, DSR90] and a Galerkin Least-Squares scheme [Bar93] are shown in Figures 8 and 9. As can be seen, the combination of the nonlinear upwind scheme of Equation 15 and the linear reconstruction give superior results for this problem.

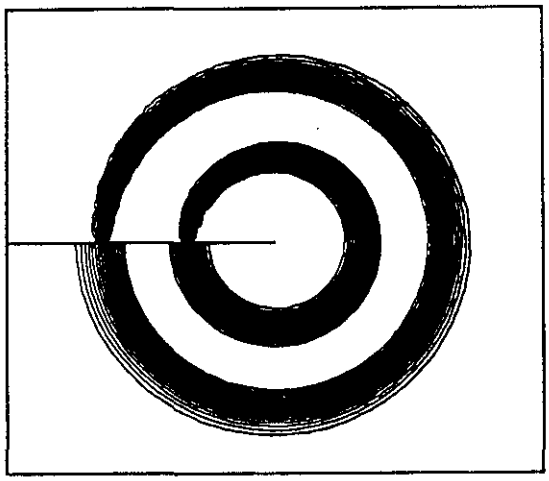

Figure 6: Circular Convection Results — Upwind Scheme with Reconstruction

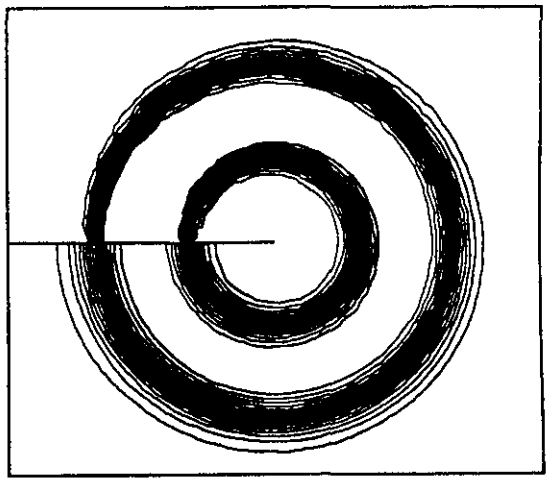

Figure 8: Circular Convection Results — Fluctuation-Splitting NN Scheme

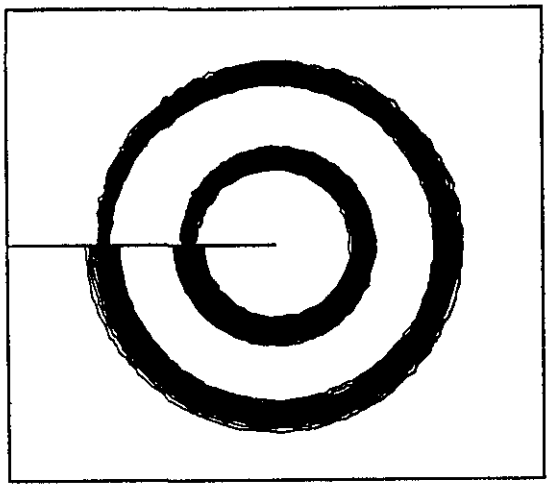

Figure 7: Circular Convection Results — Nonlinear Upwind Scheme with Reconstruction

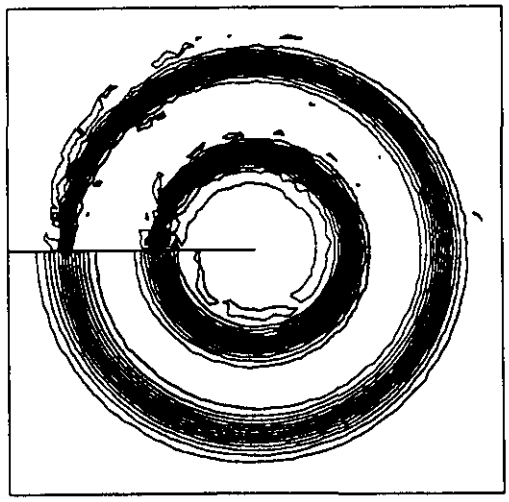

Figure 9: Circular Convection Results — Galerkin Least-Squares Scheme

The Wave Models

The Euler equations in two dimensions may be written as

$$\mathbf{U}_t + \mathbf{F}_x + \mathbf{G}_y = 0 \tag{16}$$

where

$$\mathbf{U} = \begin{bmatrix} \rho \\ \rho u \\ \rho v \\ \rho E \end{bmatrix} \quad \mathbf{F} = \begin{bmatrix} \rho u \\ \rho u^2 + p \\ \rho uv \\ \rho uH \end{bmatrix} \quad \mathbf{G} = \begin{bmatrix} \rho v \\ \rho uv \\ \rho v^2 + p \\ \rho vH \end{bmatrix}$$

Wave-like solutions, of the form

$$\begin{aligned} \mathbf{U} &= \mathbf{U}(\mathbf{k}\cdot\mathbf{x} - \lambda t) \\ &= \mathbf{U}(\xi) \end{aligned}$$

may be sought, with $\mathbf{k}$ and $\mathbf{x}$ defined as

$$\begin{aligned} \mathbf{k} &= \begin{bmatrix} \cos\theta \\ \sin\theta \end{bmatrix} \\ \mathbf{x} &= \begin{bmatrix} x \\ y \end{bmatrix}. \end{aligned}$$

This leads to the eigenvalue problem

$$[\mathbf{A}\cos\theta + \mathbf{B}\sin\theta - \lambda\mathbf{I}]\,\mathbf{U}'(\xi) = 0\,, \tag{17}$$

where $\mathbf{A}$ and $\mathbf{B}$ are the Jacobian matrices

$$\mathbf{A} = \frac{\partial \mathbf{F}}{\partial \mathbf{U}} \qquad \mathbf{B} = \frac{\partial \mathbf{G}}{\partial \mathbf{U}}\,.$$

This eigenvalue problem admits non-trivial solutions only if $\mathbf{U}'(\xi)$ is a right eigenvector of $(\mathbf{A}\cos\theta + \mathbf{B}\sin\theta)$, with λ its corresponding eigenvalue. These eigenvectors represent a shear wave, an entropy wave, and two acoustic waves. The waves propagate in the direction of the $\mathbf{k}$ unit vector. The eigenvalues represent the speed of propagation of the waves.

Discrete wave models for the Euler equations are based on a local decomposition of the solution gradient by projection onto these eigenvectors. Two discrete wave models which have been previously developed will be tested in the scheme presented here. The first decomposes residuals into two shear waves, two acoustic waves and an entropy wave [PM92]; the second uses four acoustic waves, a shear wave and an entropy wave. The angles associated with the waves of the first model are

$$\begin{aligned} \theta_{en} &= \tan^{-1}\frac{a^2\rho_y - p_y}{a^2\rho_x - p_x} \\ \theta_{ac_1} &= \tan^{-1}\frac{p_y}{p_x} \\ \theta_{ac_2} &= \theta_{ac_1} + \pi \\ \theta_{sh_1} &= \frac{1}{2}\tan^{-1}\frac{(v_y - u_x) - \cos 2\theta_{ac_1}\,(u_x + v_y)}{(v_x + u_y) + \sin 2\theta_{ac_1}\,(u_x + v_y)} \\ \theta_{sh_2} &= \theta_{sh_1} + \frac{\pi}{2}\,. \end{aligned} \tag{18}$$

The strengths of the waves are given by

$$\begin{aligned} \alpha_{en} &= \frac{1}{\rho a^2}\sqrt{(a^2\rho_x - p_x)^2 + (a^2\rho_y - p_y)^2} \\ \alpha_{ac_1} &= \frac{1}{2\rho a^2}\left[\sqrt{p_x^2 + p_y^2} + \rho a \nabla\cdot\mathbf{u}\right] \\ \alpha_{ac_2} &= \frac{1}{2\rho a^2}\left[\sqrt{p_x^2 + p_y^2} - \rho a \nabla\cdot\mathbf{u}\right] \\ \alpha_{sh_1} &= \frac{1}{2a}[(v_x - u_y) - \\ &\quad ((v_x + u_y) + \nabla\cdot\mathbf{u}\sin 2\theta_{ac_1})\cos 2\theta_{ac_1} + \\ &\quad ((v_y - u_x) - \nabla\cdot\mathbf{u}\cos 2\theta_{ac_1})\sin 2\theta_{ac_1}] \\ \alpha_{sh_2} &= \frac{1}{2a}[(v_x - u_y) + \\ &\quad ((v_x + u_y) + \nabla\cdot\mathbf{u}\sin 2\theta_{ac_1})\cos 2\theta_{ac_1} + \\ &\quad ((v_y - u_x) - \nabla\cdot\mathbf{u}\cos 2\theta_{ac_1})\sin 2\theta_{ac_1}[19) \end{aligned}$$

For the second model, the wave angles are given by

$$\begin{aligned} \theta_{en} &= \tan^{-1}\frac{a^2\rho_y - p_y}{a^2\rho_x - p_x} \\ \theta_{ac_1} &= \frac{1}{2}\tan^{-1}\frac{v_x + u_y}{u_x - v_y} \\ \theta_{ac_2} &= \theta_{ac_1} + \pi \\ \theta_{ac_3} &= \theta_{ac_1} + \frac{\pi}{2} \\ \theta_{ac_4} &= \theta_{ac_1} - \frac{\pi}{2} \\ \theta_{sh} &= \theta_{ac_1} - \frac{\pi}{4}\mathrm{sgn}\,(v_x - u_y) \end{aligned} \tag{20}$$

and the strengths are

$$\begin{aligned} \alpha_{en} &= \frac{1}{\rho a^2}\sqrt{(a^2\rho_x - p_x)^2 + (a^2\rho_y - p_y)^2} \\ \alpha_{sh} &= \frac{v_x - u_y}{a} \\ \alpha_{ac_1} &= \frac{1}{2}\left[\frac{u_x + v_y + R - a\alpha_{sh}}{2a} + \right. \\ &\qquad \left. \frac{p_x\cos\theta_{ac_1} + p_y\sin\theta_{ac_1}}{\rho a^2}\right] \\ \alpha_{ac_2} &= \frac{1}{2}\left[\frac{u_x + v_y - R - a\alpha_{sh}}{2a} - \right. \\ &\qquad \left. \frac{p_x\sin\theta_{ac_1} - p_y\cos\theta_{ac_1}}{\rho a^2}\right] \\ \alpha_{ac_3} &= \frac{1}{2}\left[\frac{u_x + v_y + R + a\alpha_{sh}}{2a} - \right. \\ &\qquad \left. \frac{p_x\cos\theta_{ac_1} + p_y\sin\theta_{ac_1}}{\rho a^2}\right] \\ \alpha_{ac_4} &= \frac{1}{2}\left[\frac{u_x + v_y - R + a\alpha_{sh}}{2a} + \right. \\ &\qquad \left. \frac{p_x\sin\theta_{ac_1} - p_y\cos\theta_{ac_1}}{\rho a^2}\right] \end{aligned} \tag{21}$$

where

$$R = \sqrt{(v_x + u_y)^2 + (u_x - v_y)^2}\,.$$

For each of the schemes, the eigenvectors associated with the various waves are given by

$$\begin{aligned}
\mathbf{R}_{en} &= \left[\rho, \rho u, \rho v, \frac{1}{2}\left(u^2 + v^2\right)\right]^T \\
\mathbf{R}_{ac} &= [\rho, \rho\left(u + a\cos\theta_{ac}\right), \rho\left(v + a\sin\theta_{ac}\right), \\
&\qquad \rho\left(H + a\left(u\cos\theta_{ac} + v\sin\theta_{ac}\right)\right)]^T \\
\mathbf{R}_{sh} &= [0, -\rho a\sin\theta_{sh}, \rho a\cos\theta_{sh}, \\
&\qquad \rho a\left(v\cos\theta_{sh} - u\sin\theta_{sh}\right)]^T \qquad (22)
\end{aligned}$$

and the eigenvalues are

$$\begin{aligned}
\lambda_{en} &= u\cos\theta + v\sin\theta \\
\lambda_{ac} &= u\cos\theta + v\sin\theta + a \\
\lambda_{sh} &= u\cos\theta + v\sin\theta\,. \qquad (23)
\end{aligned}$$

The Flux Function

For a two-dimensional scalar conservation law

$$u_t + f_x + g_y = 0$$

with

$$f = \lambda_x u \qquad g = \lambda_y u$$

and

$$\phi = (f, g)\cdot\mathbf{n}\,,$$

the flux function corresponding to first-order upwind differencing may be written as

$$\begin{aligned}
\phi\left(u_L, u_R\right) &= \frac{1}{2}\left(\left(f_L, g_L\right)\cdot\mathbf{n} + \left(f_R, g_R\right)\cdot\mathbf{n}\right) - \\
&\qquad \frac{1}{2}\left|\lambda\right|\Delta u \\
&= \frac{1}{2}\left(\left(f_L, g_L\right)\cdot\mathbf{n} + \left(f_R, g_R\right)\cdot\mathbf{n}\right) - \\
&\qquad \frac{1}{2}\left|\lambda\right|\nabla u\cdot\mathbf{dx} \qquad (24)
\end{aligned}$$

where $\mathbf{n}$ is the normal to the face, and $\mathbf{dx}$ is the vector from the left cell center to the right cell center. That is, the solution gradient is projected onto the $\mathbf{dx}$ vector, and the convection speed is projected onto the face normal, and its absolute value taken.

For a wave-model-based scheme, in which the solution gradient is expressed as the sum of waves, i.e.

$$\nabla\mathbf{U} = \sum_m \alpha_m \mathbf{R}_m \mathbf{k}_m \qquad (25)$$

where the m^{th} wave moves in direction $\mathbf{k}_m$ with speed λ_m, the corresponding flux function may be written as [PM92]

$$\begin{aligned}
\boldsymbol{\Phi}\left(\mathbf{U}_L, \mathbf{U}_R\right) &= [\mathbf{F}, \mathbf{G}]\cdot\mathbf{n}\left(\mathbf{U}_L, \mathbf{U}_R\right) \qquad (26) \\
&= \frac{1}{2}\left(\left[\mathbf{F}_L, \mathbf{G}_L\right]\cdot\mathbf{n} + \left[\mathbf{F}_R, \mathbf{G}_R\right]\cdot\mathbf{n}\right) - \\
&\qquad \frac{1}{2}\sum_m \left|\lambda_m\mathbf{k}_m\cdot\mathbf{n}\right|\,\mathbf{k}\cdot\mathbf{t}\,\alpha_m\mathbf{R}_m \qquad (27)
\end{aligned}$$

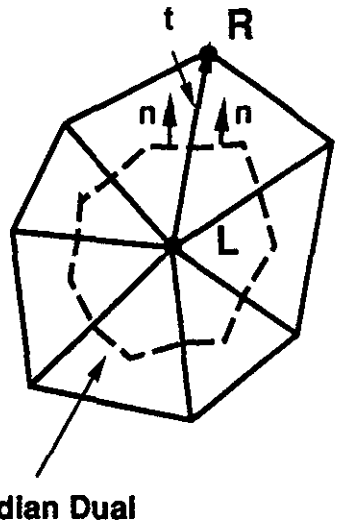

Figure 10: Vertex Mesh and the Median Dual

In the above, L and R correspond to the two nodes defining an edge in the mesh, and $\mathbf{n}$ is the normal to the piece of the median dual inside the triangle in which the gradient is calculated and decomposed (see Figure 10), and $\mathbf{t}$ is the vector connecting L and R. This flux function expresses the analogous scheme for a system of equations to the scalar scheme of Equation 15. Because the wave speeds and directions are calculated from the solution gradient, they correspond to the projected wave speeds, $\boldsymbol{\lambda}^*$ of the scalar scheme.

Flux Summation and Time Integration

The fluxes are summed for all of the faces of a cell in the median dual; the resulting residual is attributed to the vertex associated with that dual cell. The changes are integrated in time using a multi-stage procedure. A four-stage Runge-Kutta scheme was used for the results presented in this paper, with local time-stepping.

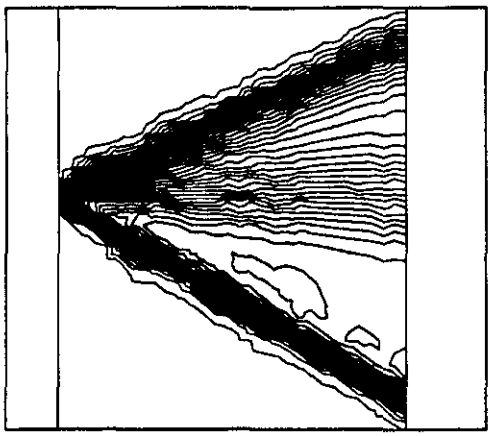

Figure 11: First-Order Grid-Aligned Solution for Interacting Streams

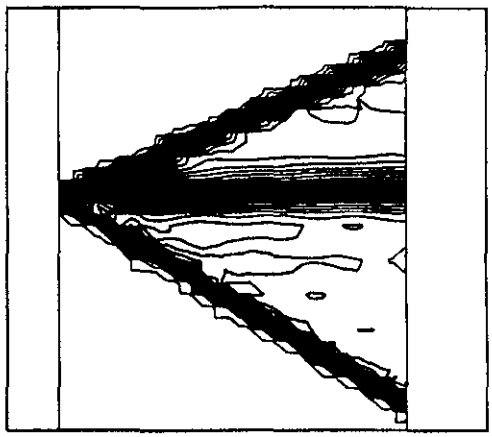

Figure 12: Second-Order Grid-Aligned Solution for Interacting Streams

Results and Discussion

Three test cases were used to assess the schemes. The first is the interaction of two supersonic streams, the second is subcritical flow past an airfoil, and the third is supercritical flow past an airfoil.

Interacting Supersonic Streams

In this case, two supersonic streams enter from the left side of the domain: the top stream has $\rho = 1.0$, $u = 2.5$, $v = -1.0$ and $p = 1.0$; the bottom stream has $\rho = 1.0$, $u = 2.0$, $v = 1.0$ and $p = 1.0$. Velocity contours for a first-order grid-aligned upwind scheme and a second-order grid-aligned upwind scheme are shown in Figures 11 and 12. The two oblique shocks, and the shear/contact, are captured with much less diffusion by the higher-order scheme.

The results of the wave-model-based scheme are shown in Figures 13 and 14. Although, strictly speaking, the wave-model-based scheme is first order, the results compare favorably with the second-order grid-aligned results. The ways in which the wave models interpret the shocks and shear/contact can be seen in Figures 15–18. These are plots of contours of wave strengths, showing the regions in which the wave models interpret specific waves as being particularly important. The four-acoustic-wave model has basically zero wave strengths for the first two acoustic waves, non-zero strengths in *one* of the shocks for the third acoustic wave (Figure 15), and non-zero strengths in the *other* shock for the fourth acoustic wave (Figure 16). This is consistent with the physics of the flow; the shocks are seen as primarily acoustic disturbances, and the model differentiates between the two shocks. The two-acoustic-wave model has non-zero acoustic waves in the shocks (Figure 17), but does not differentiate between the two shocks; *both* acoustic waves have non-zero strengths in *both* shocks. The four-acoustic-wave model also does a somewhat better job interpreting the shear; the shear wave strength, shown in Figure 18, is near zero in the shocks, and appreciable in the shear/contact. In the two-acoustic-wave model, strengths are appreciable in the shocks and the shear/contact. Thus it seems that, while both wave models give non-zero wave strengths only where they should (i.e. in the shocks and the shear/contact), the four-acoustic-wave model does a better job of separating out the effects of shear and acoustic waves.

Subcritical Airfoil Case

For this case, a NACA 0012 airfoil at 2° angle of attack in a Mach 0.63 stream was used. Mach contours for a second-order grid-aligned scheme are shown in Figure 19; the Mach contours for the two-acoustic-wave and four-acoustic-wave models are shown in Figures 20 and 21. Results from a standard Galerkin least-squares scheme, and a Galerkin least-squares scheme in which the four-acoustic-wave model is used to construct the stabilizing terms [Bar93] are shown in Figures 23 and 24. Qualitatively, the solutions are quite similar. A quantitative comparison of the C_p's computed by the various methods is shown in Figure 22. The two wave-model-based schemes lie

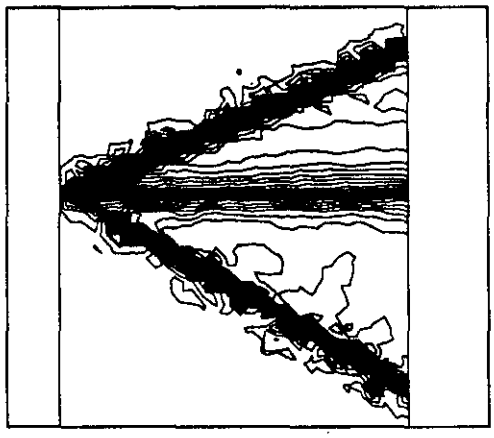

Figure 13: Two-Acoustic Wave Model Solution for Interacting Streams

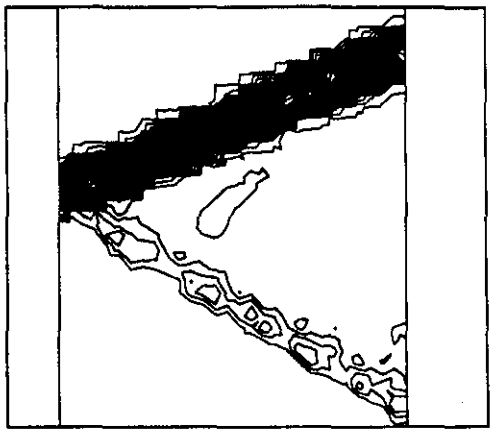

Figure 15: Four-Acoustic Wave Model for Interacting Streams — Acoustic 3 Strength

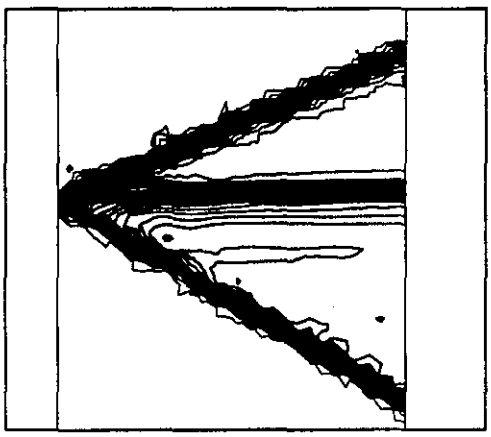

Figure 14: Four-Acoustic Wave Model Solution for Interacting Streams

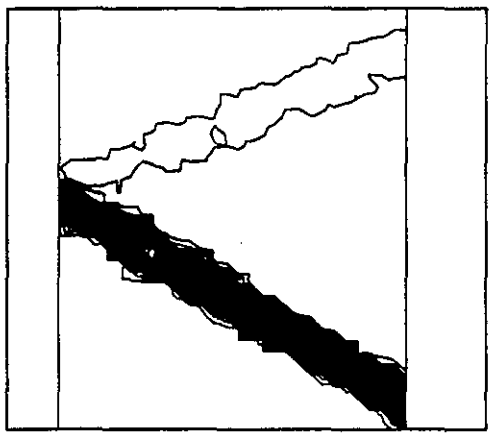

Figure 16: Four-Acoustic Wave Model for Interacting Streams — Acoustic 4 Strength

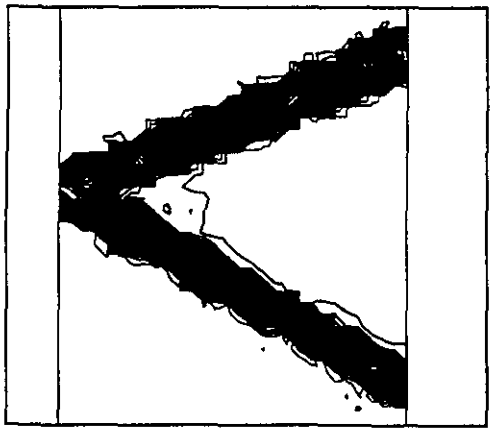

Figure 17: Two-Acoustic Wave Model for Interacting Streams — Acoustic-Wave Strength

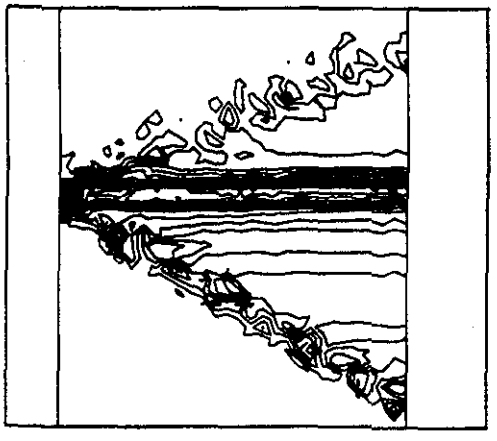

Figure 18: Four-Acoustic Wave Model for Interacting Streams — Shear Wave Strength

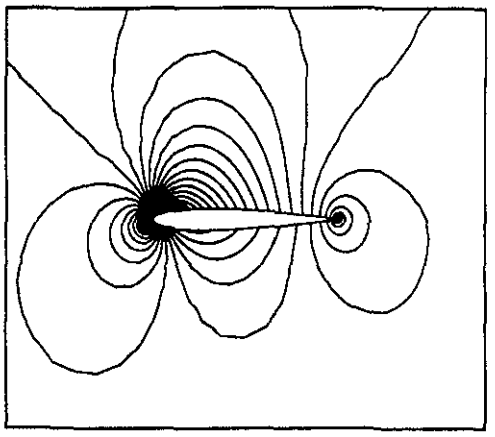

Figure 19: Second-Order Grid-Aligned Solution for Subcritical Airfoil

between the first-order and second-order grid-aligned results. The Galerkin results, which are not included in the plot, correspond quite closely to the second-order result (the standard Galerkin least-squares scheme) and the four-acoustic-wave result (the wave-model-based Galerkin scheme). Wave-strength plots for this case are less instructive than for the previous case; all of the wave strengths are non-zero at the leading and trailing edges, and zero elsewhere. The results of the wave-model-based schemes are disappointing for this case; the use of the wave model actually *deteriorates* the results of the Galerkin scheme, and the new flux function does not perform particularly well with either wave model.

Supercritical Airfoil Case

For this case, a NACA 0012 airfoil at 1.25° angle of attack in a Mach 0.8 stream was used. Mach contours for a second-order grid-aligned scheme are shown in Figure 25. The Mach contours for the two-acoustic-wave and four-acoustic-wave models are shown in Figures 26 and 27; the Mach contours for the standard and wave-model-based Galerkin least squares approaches are shown in Figures 29 and 30 for comparison. For this case, the two-acoustic-wave model has problems capturing the expansion correctly; expansion shocks form near the sonic line. The four-acoustic-wave model gives a result that compares favorably with the second-order grid-aligned solution, although there are some oscillations upstream of the upper-surface shock, and the lower-surface shock is not captured well. A comparison of the surface C_p's is

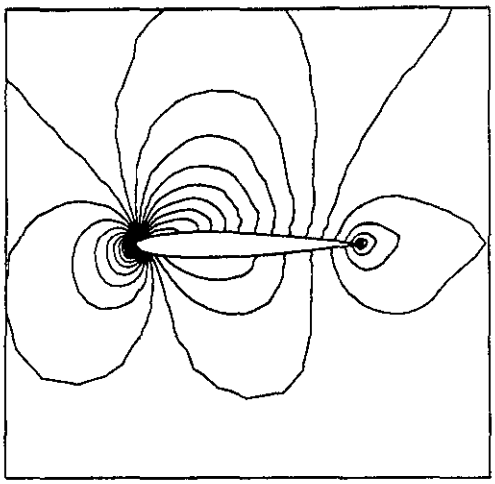

Figure 20: Two-Acoustic-Wave Model Solution for Subcritical Airfoil

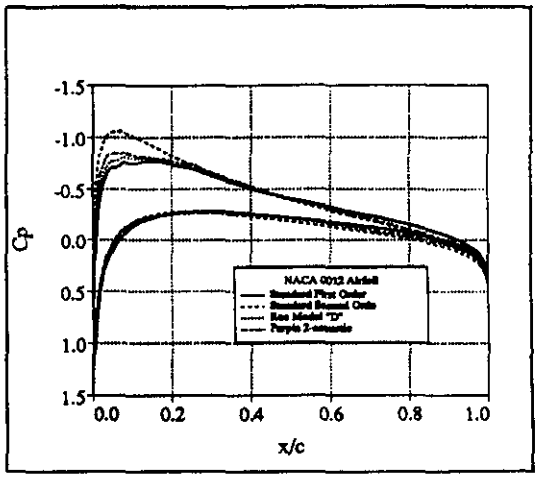

Figure 22: Comparison Solutions for Subcritical Airfoil

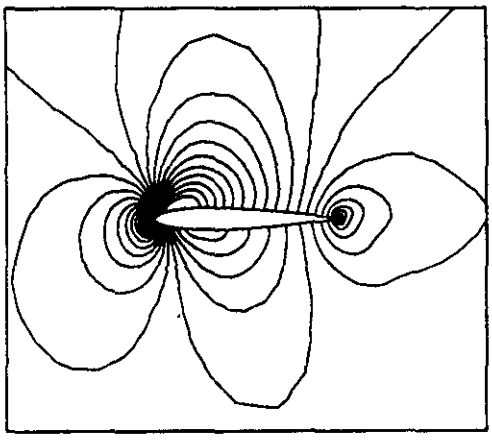

Figure 21: Four-Acoustic-Wave Model Solution for Subcritical Airfoil

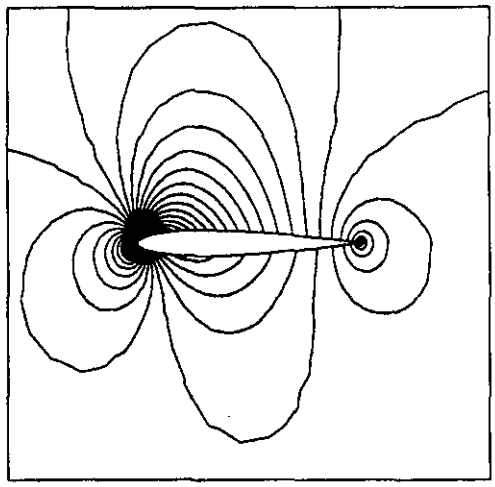

Figure 23: Galerkin Least-Squares (Standard) Solution for Subcritical Airfoil

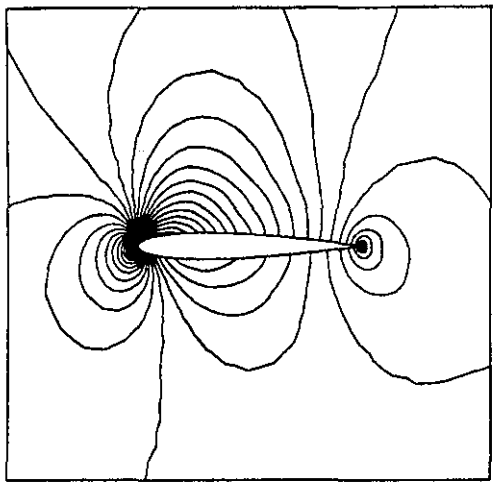

Figure 24: Galerkin Least-Squares (Wave-Model-Based) Solution for Subcritical Airfoil

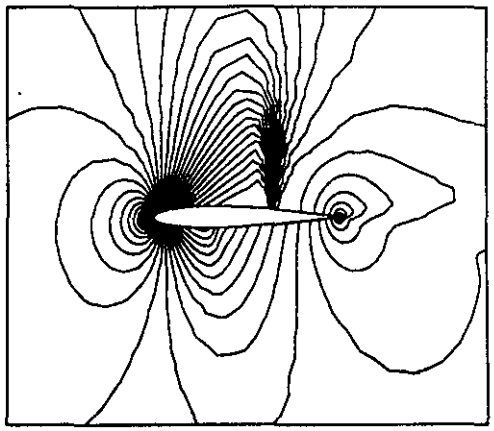

Figure 25: Second-Order Grid-Aligned Solution for Supercritical Airfoil

shown in Figure 28. The results of the four-acoustic-wave model lie between the first-order and second-order grid-aligned results. The standard Galerkin least squares approach behaves extremely well for this problem. The Galerkin least squares approach with the wave-model-based damping does not fare as well; there are oscillations upstream of the upper-surface shock.

Sample wave strengths for the two-acoustic-wave model are shown in Figures 31–32. These are charateristic of all of the wave strengths in both models, in that the leading and trailing edges and the upper-surface shock are the dominant features. They point out a shortcoming of the wave-model-based schemes, however; the leading-edge is interpreted as a region of strong acoustic waves. This leads to substantial damping in this region.

Concluding Remarks

The results presented in this paper simultaneously suggest that there is potential for a scheme using a flux function based on a wave model and scalar advection to outperform standard MUSCL schemes, and that this potential has not yet been realized. Each piece works well on its own: witness the scalar advection performance shown in Figure 5 and the performance of the four-acoustic-wave model demonstrated in the interacting supersonic streams case. The performance on the airfoil cases remains disappointing, however. It looks as though the wave models are the primary culprit. In a case like the supersonic in-

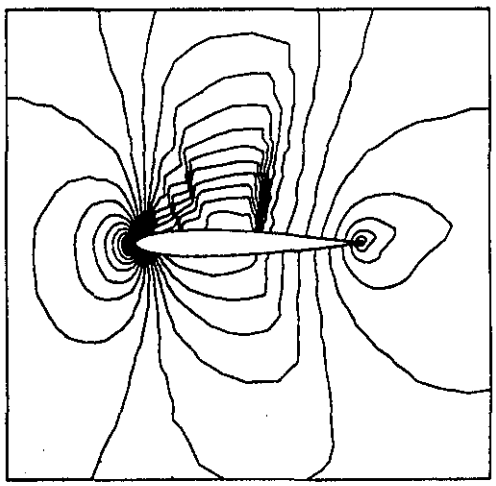

Figure 26: Two-Acoustic-Wave Model Solution for Supercritical Airfoil

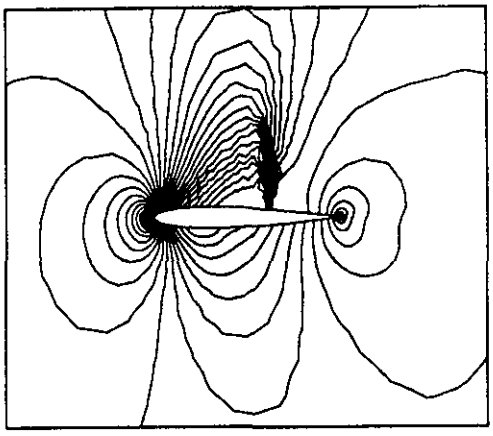

Figure 27: Four-Acoustic-Wave Model Solution for Supercritical Airfoil

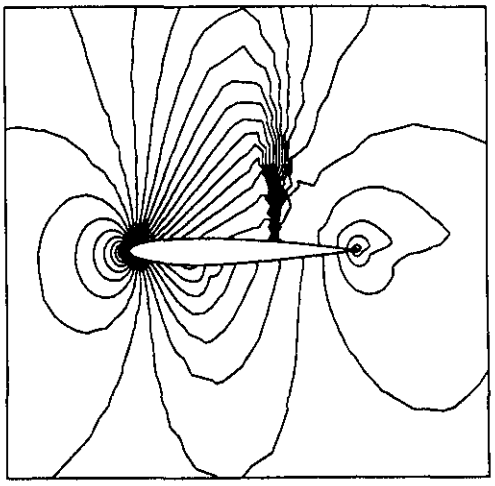

Figure 29: Galerkin Least-Squares (Standard) Solution for Supercritical Airfoil

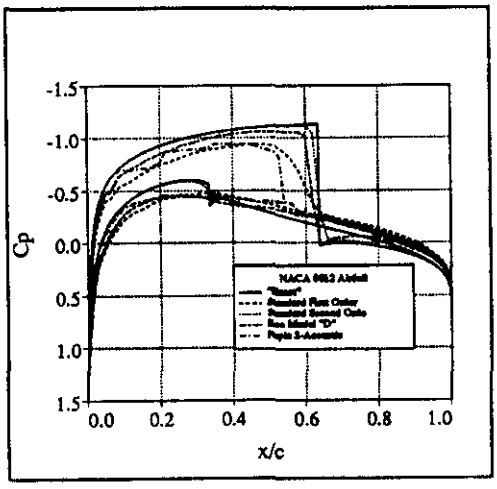

Figure 28: Comparison Solutions for Supercritical Airfoil

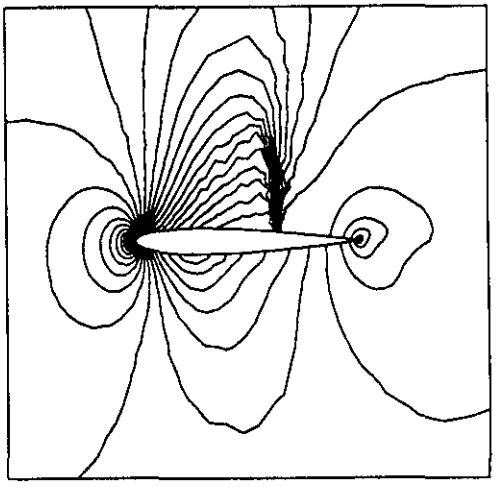

Figure 30: Galerkin Least-Squares (Wave-Model-Based) Solution for Supercritical Airfoil

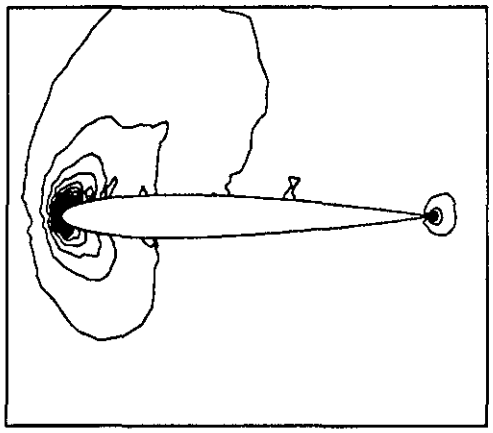

Figure 31: Four-Acoustic Wave Model for Supercritical Airfoil — Acoustic 2 Strength

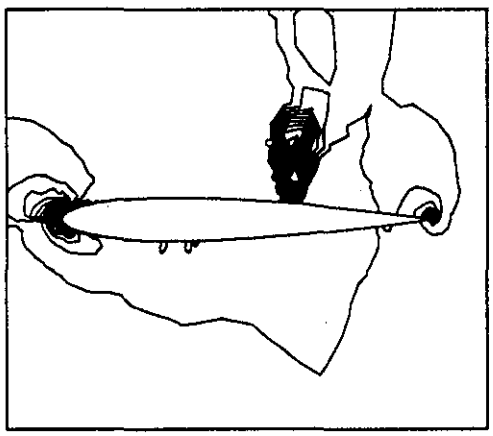

Figure 32: Four-Acoustic Wave Model for Supercritical Airfoil — Acoustic 3 Strength

teracting streams, the wave models, particularly the four-acoustic model, do a good job of interpreting the data. In more complicated cases, they do not perform as well. In particular, stagnation points are not well interpreted by the wave models, leading to overdamping of these regions. Also, the wave models seem to lead to an underdamping of portions of the flow in the transonic airfoil case, enough to lead to expansion shocks in the two-acoustic-wave model.

Attempts at extending the Euler solver to higher accuracy by use of a reconstruction step have not yet been successful. In the scalar case, this extension is straightforward, and the results are impressive, as shown in Figure 5. The extension for the system of equations is far from straightforward, and has yet to lead to results that are appreciably better than the ones presented here.

The scheme presented in this paper is very modular; it makes use of the fact that a multi-dimensional wave model is available, but is not tied to a specific model. With further work on the development of multi-dimensional wave models, and on the incorporation of a reconstruction step to make these schemes higher order, a marked improvement in results should be able to be achieved.

References

[Bar90] T. J. Barth. On unstructured grids and solvers. In *Computational Fluid Dynamics*. Von Kármán Institute for Fluid Dynamics, Lecture Series 1990-04, 1990.

[Bar93] T. J. Barth. Recent developments in high-order k-exact reconstruction on unstructured meshes. AIAA Paper 93-0668, 1993.

[BF90] T. J. Barth and P. O. Frederickson. Higher order solution of the Euler equations on unstructured grids using quadratic reconstruction. AIAA Paper 90-0013, 1990.

[DSPR91] H. Deconinck, R. Struijs, K. Powell, and P. Roe. Multi-dimensional schemes for scalar advection. In *AIAA 10th Computational Fluid Dynamics Conference*, 1991.

[DSR90] H. Deconinck, R. Struijs, and P. L. Roe. Fluctuation splitting for multi-dimensional convection problems: An alternative to finite-volume and finite-element methods. In *Computational Fluid Dynamics*. Von Kármán Institute for Fluid Dynamics, Lecture Series 1990-04, 1990.

[PM92] I. H. Parpia and D. J. Michalek. A nearly-monotone genuinely multi-dimensional scheme for the Euler equations. AIAA Paper 92-035, 1992.

[PvLR90] K. G. Powell, B. van Leer, and P. L. Roe. Towards a geunuinely multi-dimensional upwind scheme. In *Computational Fluid Dynamics.* Von Kármán Institute for Fluid Dynamics, Lecture Series 1990-04, 1990.

[RS91] P. L. Roe and D. Sidilkover. Optimum positive linear schemes for advection in two and three dimensions. Submitted to *Journal of Computational Physics*, 1991.

[SDD+91] R. Struijs, H. Deconinck, P. DePalma, P. Roe, and K. Powell. Progress on multi-dimensional Euler solvers on unstructured grids. In *AIAA 10th Computational Fluid Dynamics Conference*, 1991.

[Sid89] David Sidilkover. *Numerical Solution to Steady-State Problems with Discontinuities.* PhD thesis, Weizmann Institute of Science, 1989.

[vL79] B. van Leer. Towards the ultimate conservative difference scheme. V. A second-order sequel to Godunov's method. *Journal of Computational Physics*, 32, 1979.